


Article

Thermal–Mechanical Coupling Evaluation of the Panel Performance of a Prefabricated Cabin-Type Substation Based on Machine Learning

Xiangsheng Lei ¹, Jinwu Ouyang ², Yanfeng Wang ¹, Xinghua Wang ¹, Xiaofeng Zhang ³, Feng Chen ³, Chang Xia ², Zhen Liu ^{2,*}  and Cuiying Zhou ^{2,*}

¹ Power Grid Planning Research Center of Guangdong Power Grid Limited Liability Company, Guangzhou 510699, China; leixiangsheng@gd.csg.cn (X.L.); wangyanfeng@gd.csg.cn (Y.W.); wangxinghua@gd.csg.cn (X.W.)

² Guangdong Engineering Research Centre for Major Infrastructure Safety, Sun Yat-Sen University, Guangzhou 510275, China; ouyujw@mail2.sysu.edu.cn (J.O.); xiach9@mail2.sysu.edu.cn (C.X.)

³ China Energy Construction Group Guangdong Electric Power Design and Research Institute Limited Liability Company, Guangzhou 510060, China; zhangxiaofeng@gedi.com.cn (X.Z.); chenfang@gedi.com.cn (F.C.)

* Correspondence: liuzh8@mail.sysu.edu.cn (Z.L.); zhoucy@mail.sysu.edu.cn (C.Z.)

Abstract: The panel performance of a prefabricated cabin-type substation under the impact of fires plays a vital role in the normal operation of the substation. However, current evaluations of the panel performance of substations under fire still focus on fire resistance tests, which seldom consider the relationship between fire behavior and the mechanical load of the panel under the impact of fires. Aiming at the complex and uncertain relationship between the thermal and mechanical performance of the substation panel under impact of fires, this paper proposes a machine learning method based on a BP neural network. First, the fire resistance test and the stress test of the panel is carried out, then a machine learning model is established based on the BP neural network. According to the collected data, the model parameters are obtained through a series of training and verification processes. Meanwhile, the correlation between the panel performance and fire resistance was obtained. Finally, related parameters are input into the thermal–mechanical coupling evaluation model for the substation panel performance to evaluate the fire resistance performance of the substation panel. To verify the correctness of the established model, numerical simulation of the fire test and stress test of the panel is conducted, and numerical simulation samples are predicted by the trained model. The results show that the prediction curve of neural network is closer to the real results compared with the numerical simulation, and the established model can accurately evaluate the thermal–mechanical coupling performance of the substation panel under fire.

Keywords: prefabricated cabin-type substation; panel; BP neural network; thermal–mechanical coupling; machine learning; fire behavior; impact of fires



Citation: Lei, X.; Ouyang, J.; Wang, Y.; Wang, X.; Zhang, X.; Chen, F.; Xia, C.; Liu, Z.; Zhou, C. Thermal–Mechanical Coupling Evaluation of the Panel Performance of a Prefabricated Cabin-Type Substation Based on Machine Learning. *Fire* **2021**, *4*, 93. <https://doi.org/10.3390/fire4040093>

Academic Editor: Maged Youssef

Received: 15 November 2021

Accepted: 7 December 2021

Published: 9 December 2021

Publisher's Note: MDPI stays neutral with regard to jurisdictional claims in published maps and institutional affiliations.



Copyright: © 2021 by the authors. Licensee MDPI, Basel, Switzerland. This article is an open access article distributed under the terms and conditions of the Creative Commons Attribution (CC BY) license (<https://creativecommons.org/licenses/by/4.0/>).

1. Introduction

With the development of the national economy, the demand for electricity, from all walks of life, has increased. After a period of rapid development, large-scale centralized new energy power generation has gradually extended in the direction of decentralization and miniaturization. The requirements of new energy construction cannot be met by conventional transmission substations. Technological development and the improvement of prefabricated substations have become increasingly prominent. As a new type of prefabricated substation [1–3], the prefabricated cabin-type substation is becoming an important development direction benefiting from its high degree of integration and high level of intensiveness. Fire has an important effect on the safety of buildings and structures [4,5], thus the performance of the prefabricated substation panel under impact of fires is a guarantee of safety and plays a vital role in the normal operation of the substation. As

a structural stress component of the substation panel, at the beginning of the design, the fire safety of the panel needs to be considered to ensure the safety of the overall structure of the substation. A high temperature causes the deterioration of the mechanical properties of the substation panel material, which will bring about different degrees of damage to the substation panel. Therefore, before the construction of the substation, it is necessary to carry out a fire resistance performance test under fire on the panel to ensure the fire resistance safety of the entire project in the event of a fire. Therefore, accurately describing the fire performance of substation panels has become an important issue for the stability of current substations.

Since the substation panels are mainly reinforced concrete structures, the fire performance of the substation panels can refer to the fire resistance test [6–10] and numerical simulation method to analyze fire behavior. Naser and Kodur [11] conducted an experimental study on the fire behavior of composite steel girders subjected to high shear loading. Hawileh et al. [12–14] predicted the performance of concrete beams using a finite element model. Aguado et al. [15] used a 3D finite element model for predicting the fire behavior of hollow-core slabs. However, the current research on the performance of substation panels rarely considers correlations, with little consideration of the nonlinear relationship between stress performance and fire resistance under impact of fire.

The neural network, a method of machine learning, is widely used in various fields [16–23]. Abuodeh et al. [24,25] used machine learning techniques to predict behavior of RC beams and compressive strength of ultra-high-performance concrete. Liu et al. [26] established machine-learning-based models to predict shear transfer strength of concrete joints. The neural network also has a precedent in the application of substation [27–31]. Da Silva et al. [32] proposed the use of artificial neural networks to solve the problem of fault location in substations; Wang et al. [33] used deep learning methods to identify the switch status of substations; Jiang Hongyu et al. [34] proposed an adaptive suppression method of transformer noise in substations based on genetic wavelet neural networks for the problem of transformer noise control; Oliveira et al. [35] carried out automatic monitoring on the construction site of substations based on deep learning. Neural networks [36–38] with self-learning, self-organization, and extremely strong linear fidelity capabilities can accurately reflect the nonlinear relationship between input and output variables to maintain high accuracy in short-term prediction. Therefore, machine learning is used to establish a non-linear relationship between panel stress and fire resistance from the perspective of thermal–mechanical coupling, which is a worthwhile means for evaluating the performance of substation panels under impact of fire.

To solve the above problem, this paper proposes a machine learning method based on the principle of BP (back propagation) neural networks to analyze the thermal–mechanical coupling performance of substation panels under fire. The evaluation factors are selected, such as the substation panel geometric data, mechanical performance parameters, and fire resistance performance data. After the model training ends, the relationship between panel mechanical performance and fire resistance is established. Finally, predictive samples are input into the model to evaluate the fire resistance performance of the panel. Then, fire resistance test and the stress test of the panel is carried out. A BP neural network model is trained and built through a series of training the samples. Then, numerical simulation of the fire test and stress test of the panel is conducted, and numerical simulation samples is predicted by the trained model and compared with the real results. The results show that predicted samples fit well with the actual output values and better than the result of numerical simulation. Thus, the established model can accurately evaluate the thermal–mechanical coupling performance of the panel under fire.

2. Research Methods and Contents

2.1. The Research Process for Thermal–Mechanical Coupling Evaluation of Prefabricated Cabin-Type Substation Panel Performance

The key to the thermal–mechanical coupling evaluation process of a prefabricated substation panel is to establish an evaluation model based on BP neural networks. By

inputting the stress state data of the substation panel into the evaluation model, the corresponding fire resistance parameters can be obtained. The thermal–mechanical coupling performance of the prefabricated substation panel can then be evaluated. The research process of the thermal–mechanical coupling evaluation of prefabricated substation panel performance is shown in Figure 1.

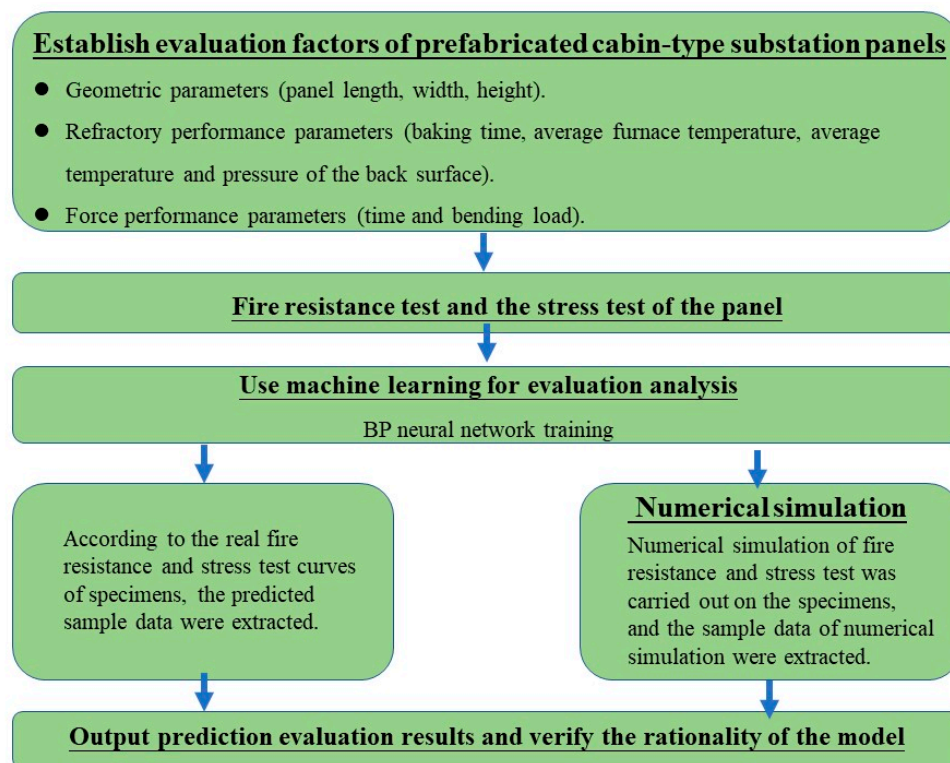


Figure 1. Research process of thermal–mechanical coupling evaluation of panel performance.

2.2. Thermal–Mechanical Coupling Evaluation Model of the Panel Performance Based on BP Neural Networks

2.2.1. Establishment of Evaluation Factors

In theory, the performance state of the prefabricated substation panel can be better described by the more comprehensive evaluation indexes. However, in practical engineering, on the one hand, it is very difficult to collect data. On the other hand, the more indexes there are, the more complex the nonlinear relationship of the thermal–mechanical coupling evaluation of the prefabricated substation panel performance is. Therefore, the determination of evaluation indexes cannot be simply generalized but should be analyzed in specific cases. As a complex system, the thermal–mechanical coupling evaluation of panel performance is affected by many factors. This study, adhering to the principles of representativeness, integrity, and desirability, takes the geometric parameters, mechanical performance, and fire resistance performance of the panel as evaluation factors of the thermal–mechanical coupling evaluation of the panel’s performance.

1. The geometric parameters of the panel include length, width, and height.
2. The fire resistance performance parameters of the panel include the heating time, average furnace temperature, average temperature of the backfire surface, and pressure parameters.
3. The mechanical performance parameters of the panel include time and bending load.

2.2.2. Construction of BP Neural Network

The BP neural network as a method of machine learning is suitable for addressing complex nonlinear problems, such as the nonlinear relationship between the mechanical

performance and the fire resistance performance of substation panels. The research process of the BP neural network model for the thermal–mechanical coupling evaluation of substation panel performance is shown in Figure 2. Firstly, the data parameters are input into the BP neural network for training. Secondly, the thermal–mechanical coupling evaluation results of the panel performance can be obtained through the model after model training. After that, we carried out numerical simulation of fire resistance test and stress test on the panel. We used the curve data of numerical simulation as sample data to predict the sample of numerical simulation. Finally, the correctness of the model is verified by comparing the real results with the numerical simulation results and the neural network prediction results.

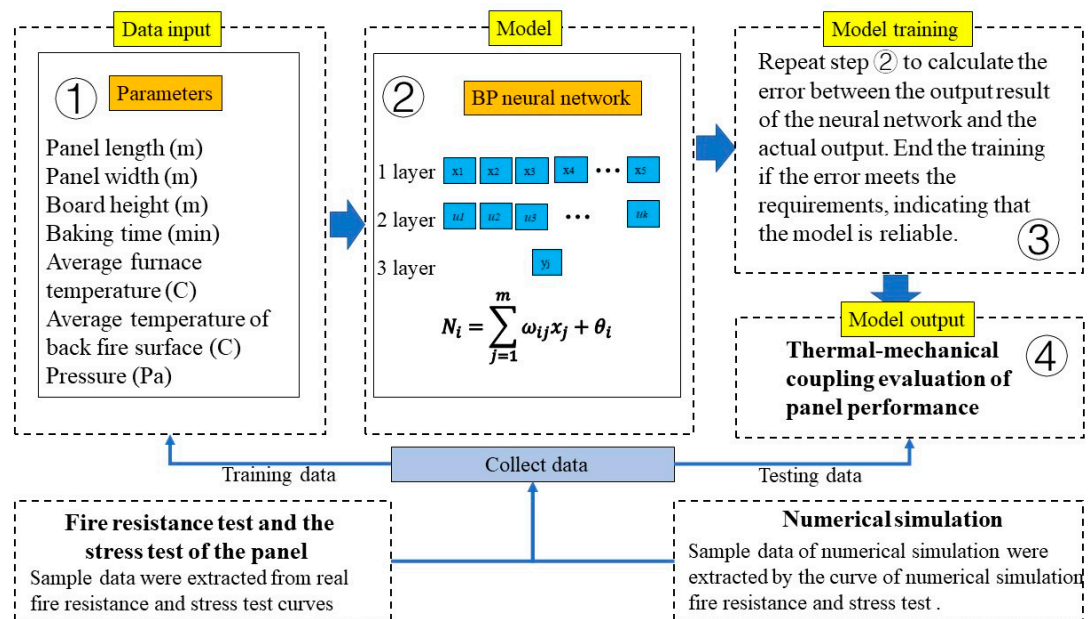


Figure 2. Research process of the BP neural network model in the thermal–mechanical coupling evaluation of prefabricated substation panel performance. x_1, x_2, \dots, x_5 , respectively, represents input layer parameters of neural network; u_1, u_2, \dots, u_k represent hidden layer parameters of the neural network, respectively; y_j represents output layer parameters of neural network; N_i represents output results of neural network; ω represents weights of neural network and θ represents thresholds of neural network.

As shown in Figure 3, the BP neural network used for the thermal–mechanical coupling evaluation training of the prefabricated cabin-type substation panel performance is composed of three layers, representing the input layer, hidden layer, and output layer, respectively.

The input layer has seven impact indicators corresponding to the identification indicators, which are the length, width, height, heating time, average furnace temperature, average temperature, and pressure of the backfire surface. The output layer represents time and bending load. Therefore, there are seven input layer nodes in this model, six hidden layer nodes, and two output nodes. Each node is a specific output function, and each connection between two nodes represents a weighted value (weight) for the signal passing through the connection. The learning rate determines the amount of weight change generated in each cycle. The fixed learning rate in this research is 0.1, the training target is 0.00001, and the maximum number of learning iterations is 100. Through repeated iterative calculations, the correlation coefficient and threshold are determined. After that, the learning and training process ends, which means the model is successfully established. After the BP neural network model training, the actual value is compared with the predicted value. In order to solve the problem of inconsistency in the units and magnitudes of the input variables in the BP neural network, normalization is used to control the sample data to 0–1.

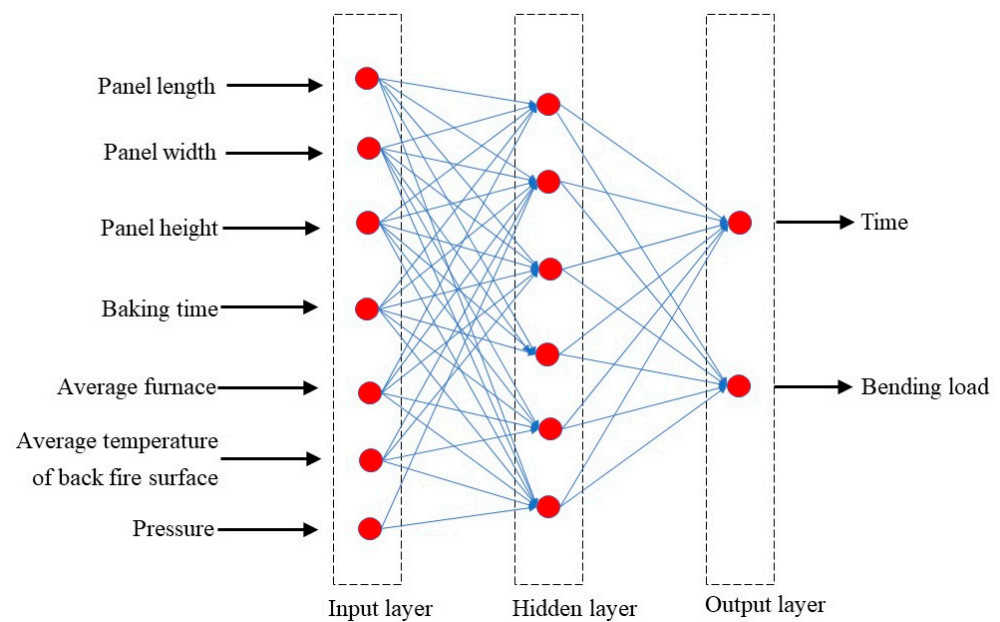


Figure 3. Application of the BP neural network in the thermal–mechanical coupling evaluation of substation panel performance.

The normalization formula is as follows:

$$Y_i = \frac{X_i - X_{min}}{X_i - X_{max}} \alpha + \beta \quad (1)$$

In the formula, X_i and Y_i represent the variables before and after normalization, respectively; X_{min} and X_{max} are the minimum and maximum values of X_i , respectively; α is a parameter with a value between 0–1, and $\beta = 1 - \frac{\alpha}{2}$.

3. Case Application Analysis

3.1. Substation Panel

3.1.1. Fire Resistance Test of Panel

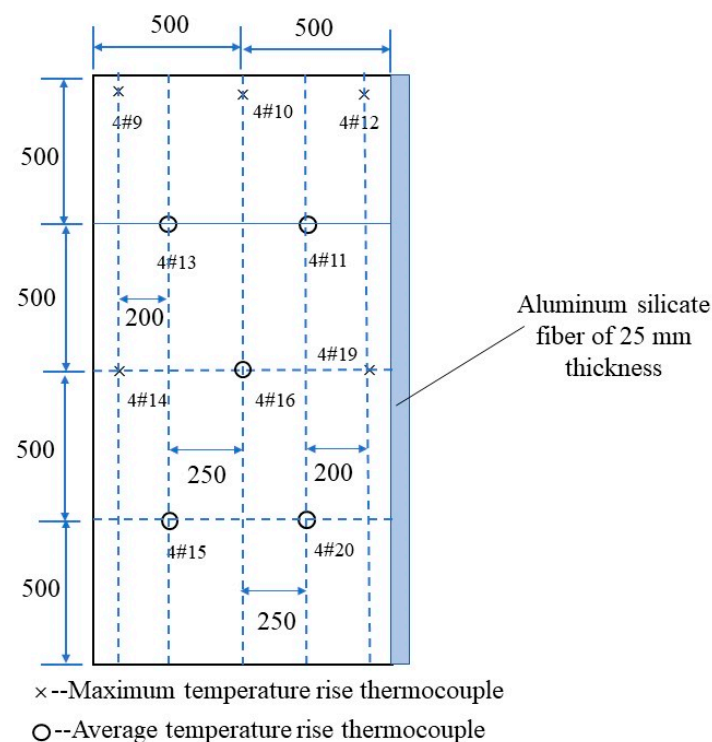
The fire resistance test of panel refer to the requirements of GB/T 9978.1-2008 “Fire resistance Test Methods for Building Components part 1: General Requirements [39]” and GB/T 9978.8-2008 “Fire resistance Test Methods for Building Components Part 8: Characteristics of non-load-bearing vertical dividers [40]”, as shown in Table 1. The test conditions and test plan were formulated according to the requirements of GB/T 9978.1-2008 [39] and GB/T 9978.8-2008 [40].

The length (m) width (m) \times height (m) of the special panel for a box-type substation is $2.0 \times 1.0 \times 0.12$. Ten temperature measurement points are set on the backfire surface of the panel with the vertical side on a free side, as shown in Figure 4.

According to the test requirements, the test uses vertical component fire test furnace device in Beijing Gequ fire test laboratory. The device can meet the requirements of the furnace temperature and pressure in Table 1. This device also can measure the temperature and pressure change value of the panel specimen. The data changes during the test can be visually displayed on the display screen of the equipment.

Table 1. Reference standards for fire resistance.

Test Items	Standard Clause	Judgment Criteria
Completeness	GB/T 9978.8-2008 Article 10 GB/T 9978.1-2008 Article 10.2.2 Article 8.4	<p>The duration of the test specimen's continuous fire resistance performance in the fire test. Any one of the following limited conditions of the test specimen shall be considered as a loss of integrity:</p> <p>(a) A cotton pad test is conducted, and the cotton pad is ignited.</p> <p>(b) A gap probe of 6 mm penetrates the specimen into the furnace and moves 150 mm along the length of the crack; a gap probe of 25 mm penetrates the specimen into the furnace.</p> <p>(c) A flame appears on the backfire surface and lasts for more than 10 s.</p>
Fire resistance		
Thermal insulation	GB/T 9978.8-2008 Article 10 GB/T 9978.1-2008 Article 10.2.3	<p>If the duration of the fire resistance and heat insulation performance of the test specimen in the fire test as well as the temperature rise of the backfire surface of the test specimen exceeds any of the following limits, it is considered to have lost the heat insulation:</p> <p>(a) The average temperature rise exceeds the initial average temperature of 140 °C.</p> <p>(b) The temperature rise at any point exceeds the initial temperature (including the moving thermocouple) by 180 °C (the initial temperature should be the initial average temperature of the back surface at the beginning of the test).</p>
	GB/T 9978.1-2008 Article 12.2.2	<p>If the "integrity" of the test specimen does not meet the requirements, it is considered that the "heat insulation" of the test specimen does not meet the requirements.</p>

**Figure 4.** Schematic diagram of the measuring point layout on the backfire surface of the test specimen.

The experiment was terminated at 181 min. The test process was observed and recorded. The test phenomena are shown in Table 2.

Table 2. Test phenomena.

Time	Observation Record
0	Test start.
30	No significant change from the previous stage.
60	No significant change from the previous stage.
90	No significant change from the previous stage.
120	Concave deformation.
150	No significant change from the previous stage.
181	Integrity and thermal insulation are undamaged; test is stopped.

The fire resistance data of the panels are shown in Figures 5 and 6.

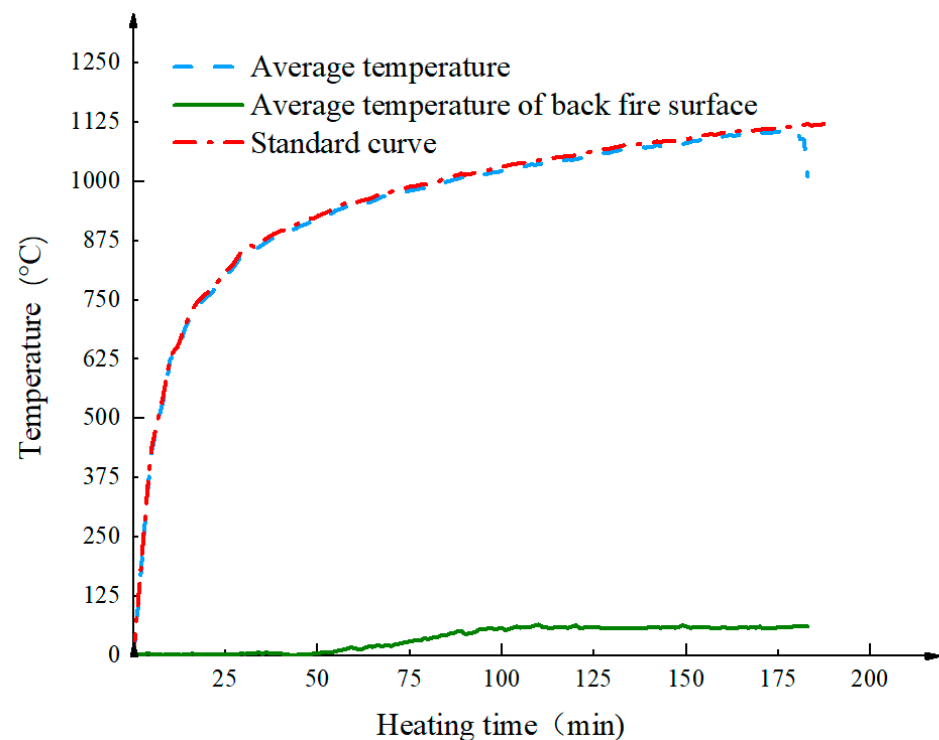


Figure 5. Temperature rise curve.

3.1.2. The Stress Test of the Panel

The same panel specimen as Section 3.1.1 was used in this experiment. Static loading is carried out by force control. A hydraulic jack was used for loading. During the test, the load is acted on the mid-span position of the panel through the actuating head. Once the specimen was destroyed, the test was over. The data of the stress test of the panel are shown in Figure 7.

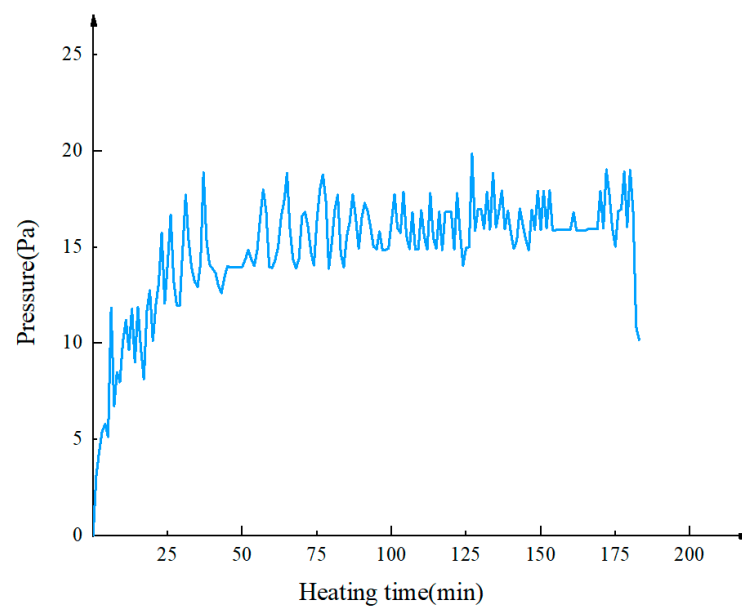


Figure 6. Pressure curve at 500 mm below the furnace roof.

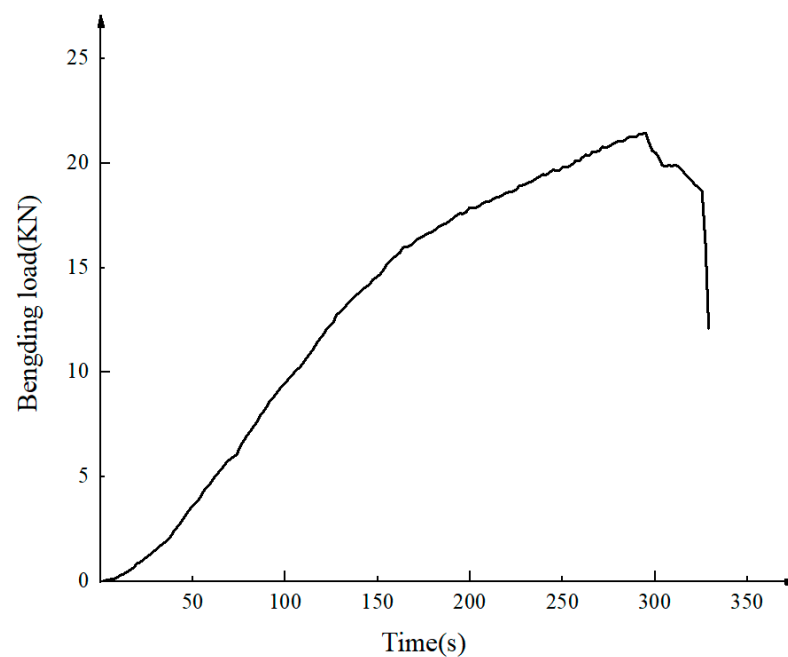


Figure 7. Stress curve of the panel strength test. Bending load refer to a load that causes bending deformation of a panel during a fixed strength test.

3.2. Thermal–Mechanical Coupling Evaluation of Panel Performance

The values were recorded every minute from the origin of the coordinates. Figures 5 and 6 show that the test specimen was damaged when heated to the 183rd minute. Figure 7 shows that the test specimen was damaged under stress at 329.052 s. The time from loading to failure was divided into 183 segments for the values recorded every 1.798 s. The fire resistance and stress performance data of the panel are shown in Appendix A. It should be emphasized that the temperature measured in Table A1 has subtract the ambient temperature. The data of columns 1 represent the number of samples; the data of columns 2 represent the heating time of panel; the data of columns 6 represent the load time of the panel.

According to the BP neural network structure constructed in Section 2.2, the thermal–mechanical coupling evaluation model of the panel performance was learned and trained:

1. Initialize the BP neural network. We randomly selected 100 sets of data from Table A1 as the input node data of the training sample, and the remaining 84 sets of data in Table A1 were used as prediction samples. Then, the weights and offsets of the neural network were initialized. Finally, the sample data were normalized.
2. Train the BP neural network. The BP neural network was used to train 100 sets of training sample data until the calculations at the end of the network training. The thermal–mechanical coupling evaluation model of the panel performance based on the BP neural network was obtained when the BP neural network converged after learning and training.
3. Predict the BP neural network. The randomly selected 84 sets of test sample data were predicted through the trained BP neural network to finally obtain the prediction result output. The graph is drawn as shown in Figure 8.

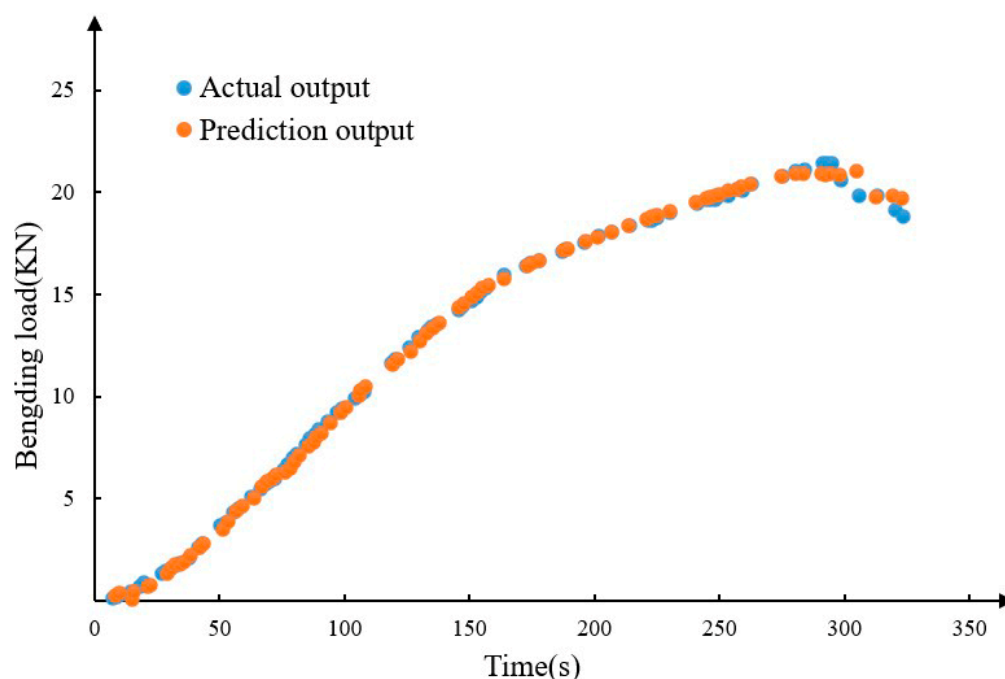


Figure 8. Comparison of sample predicted output and actual output.

It can be seen from Figure 8 that the predicted output values of the 84 groups of predicted samples fit well with the actual output values for the trend of the sample points showing basically the same, which indicates that the thermal–mechanical coupling evaluation model of panel performance based on a BP neural network is reasonable and accurate.

The mechanical performance data of the panel corresponding to the heating time of the 162nd minute to the 183rd minute were collected, as shown in Figure 9.

It can be seen from Figure 9 that, when the test specimen reaches the maximum bending load of 21.443 KN, the corresponding stress time of the substation plate is 294.888 s. When the time is 325.456 s, the bending load drops sharply from 18.664 KN, which means the material is damaged at this time. The prediction sample data of the fire resistance performance of the substation are input into the thermal–mechanical coupling evaluation model of the panel performance. The corresponding panel performance parameters can then be obtained. The test specimen reaches the maximum bending load of 21.128 KN when the predicted value of the neural network is displayed for 297.147 s. The bending load drops sharply from 18.683 KN for the material being damaged at the time of 323.658 s. By comparing the predicted value and actual value of the time and bending load, it is found that the maximum bending load and the corresponding stress time from the thermal–mechanical coupling evaluation model and actual test is very close, and the two values

essentially satisfy the error requirements. This further demonstrates the accuracy and reliability of the thermal–mechanical coupling evaluation model of the panel performance.

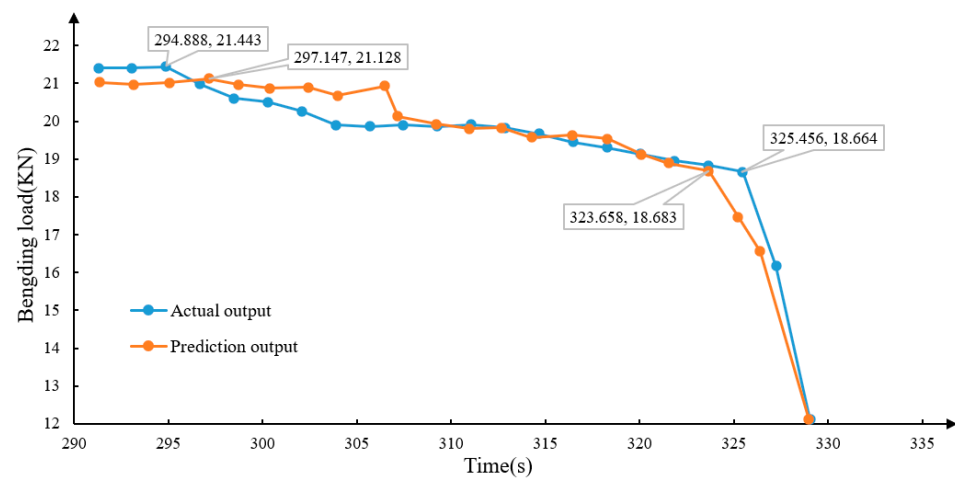


Figure 9. Sample result output of panel performance prediction.

3.3. Numerical Simulation

In order to verify the results of neural network calculation, we carried out numerical simulation on the specimen. The length (m) \times width (m) \times height (m) of the special panel for numerical simulation is $2.0 \times 1.0 \times 0.12$, as shown in Figure 10. The fire resistance test and pressure test of numerical simulation model are consistent with the actual situation in Section 3.1.

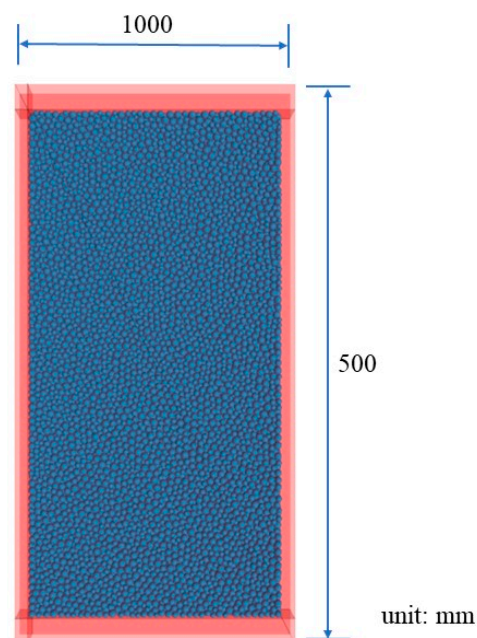


Figure 10. Numerical simulation model.

The numerical simulation results are shown in Figures 11 and 12.

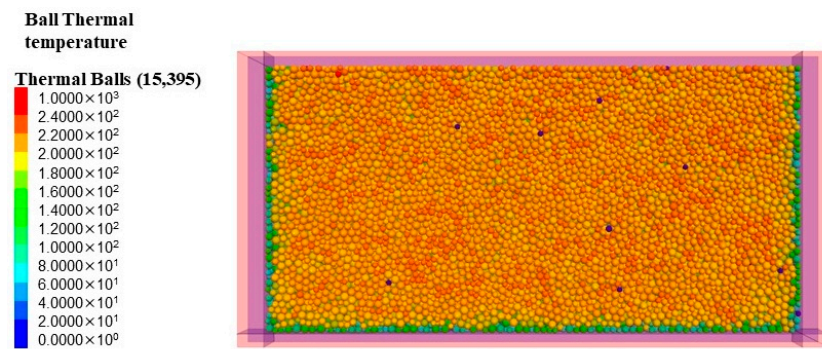


Figure 11. Numerical simulation of fire resistance test.

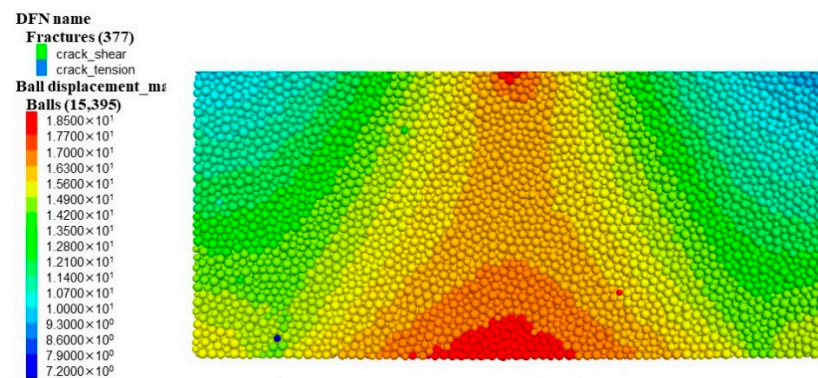


Figure 12. Numerical simulation of stress test.

The curve of the fire resistance test and pressure test parameters for the panel is shown in Figures 13 and 14. Each step in the diagram represents a unit of time.

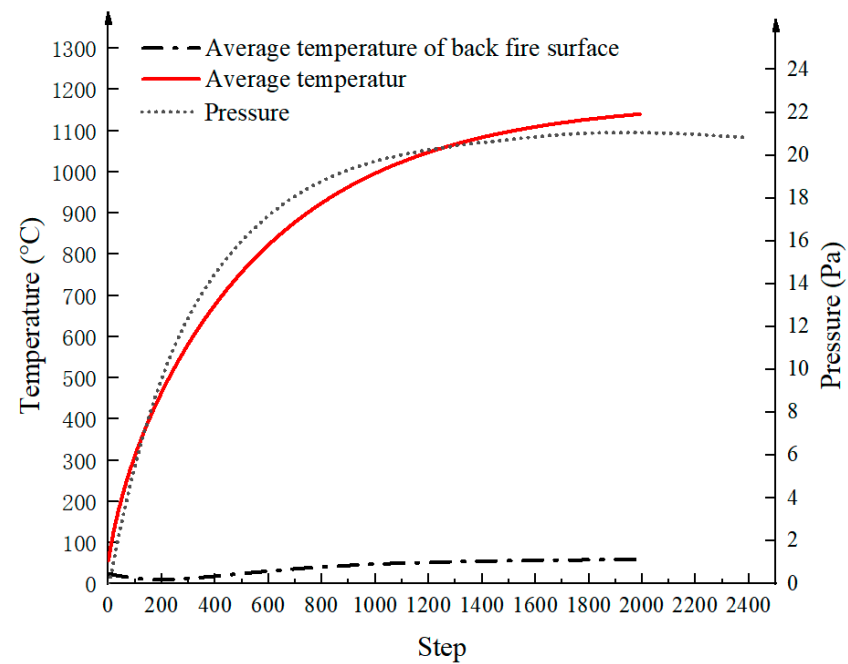


Figure 13. The curve of the fire resistance test.

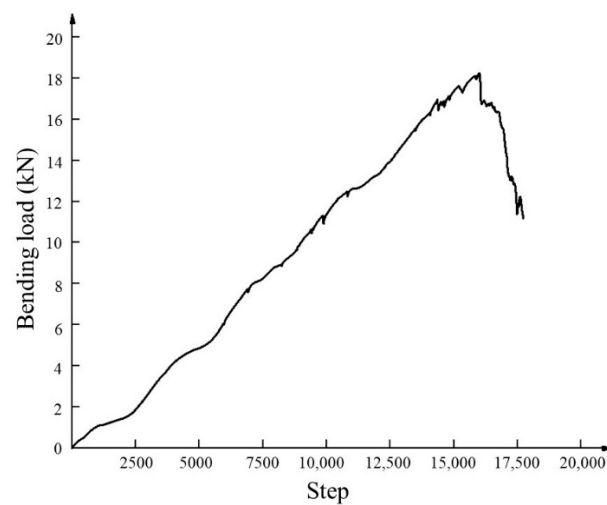


Figure 14. Stress curve of the panel samples. Bending load refer to a load that causes bending deformation of a panel during a fixed strength test.

The failure time step of numerical simulation corresponds to the failure time of fire resistance test and pressure test in real time, and the simulated result curve is also divided into 183 sections. Corresponding values are recorded in each section and 184 sample data of numerical simulation can be obtained.

According to the BP neural network structure trained in Section 3.2, we conduct neural network learning, training and prediction using the sample data of numerical simulation. According to the sample data of numerical simulation, the prediction results of numerical simulation are obtained. By converting the failure time of the real stress curve into the corresponding time step, we plotted the prediction curve of the neural network, the prediction curve of the numerical simulation and the real stress test curve in the same figure, as shown in Figure 15.

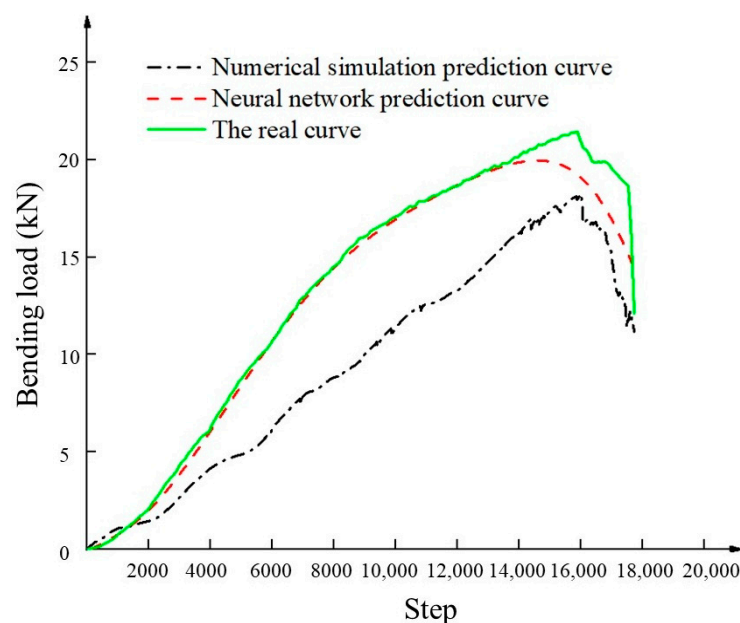


Figure 15. The stress test curve.

It can be seen from Figure 15 that the curve of prediction result of neural network and array simulation is basically consistent with the curve of real pressure test. The force increases gradually and decreases rapidly after reaching the peak value. Numerical simulation results show that when the time step is 15,850, the maximum bending load

is 18.11064 kN. The neural network prediction results show that when the time step is 14,687, the bending load reaches the maximum value of 19.963 KN. The actual test results show that when the time step is 15,889, the bending load reaches the maximum value of 21.443 kN. Compared with the results of numerical simulation, the prediction curve of neural network is closer to the real pressure curve. The percentage error of the maximum bending load calculated by numerical simulation is 15.5%, the percentage error of the maximum bending load calculated by neural network prediction is 6.9%, and the error of neural network prediction is about half smaller than that of numerical simulation. The prediction result of neural network is better than that of numerical simulation. Thus, the accuracy and rationality of the neural network prediction model can be proved.

3.4. The Functional Relationship between Fire Resistance and Stress Resistance

The relationship between the parameters of fire resistance and stress resistance can be obtained by deriving the training parameters of the neural network, as shown in Equations (2)–(5):

$$\alpha_h = \sum_{i=1}^M v_{ih}x_i + r_h \quad (2)$$

$$b_h = f(\alpha_h) \quad (3)$$

$$y_j = \sum_{h=1}^q w_{hj}b_h + \theta_j \quad (4)$$

$$f(x) = \frac{1}{1 + e^{-x}} \quad (5)$$

M refers to the number of nodes in the input layer, $M = 7$; x_i ($i = 1, 2, \dots, M$) refers to length (m), width (m), height (m), heating time (min), average furnace temperature ($^{\circ}\text{C}$), average temperature of backfire surface ($^{\circ}\text{C}$), and pressure parameter (Pa); h refers to the number of hidden layer nodes, $h = 6$; q is the number of nodes in the output layer, $q = 2$; y_j ($j = 1, 2$) refers to the values of the time (s) and bending load (KPa), respectively. v refers to weight parameters from input layer to hidden layer of neural network; r_h refers to threshold parameters from input layer to hidden layer of neural network; W refers to weight parameters from hidden layer to output layer of neural network; θ_j refers to threshold parameters from hidden layer to output layer of neural network.

$$v = \begin{bmatrix} 0 & 0 & 0 & 4.4136 & -1.6295 & -0.0460 & -0.1070 \\ 0 & 0 & 0 & 0.8386 & -0.7978 & -2.0962 & 0.1305 \\ 0 & 0 & 0 & -1.4522 & -1.0707 & -0.3682 & -0.0326 \\ 0 & 0 & 0 & 0.1633 & -0.3356 & -0.6002 & -0.0347 \\ 0 & 0 & 0 & 1.0436 & -0.0877 & -0.4381 & -0.0416 \\ 0 & 0 & 0 & 1.1642 & -0.2854 & -0.3663 & 0.1397 \end{bmatrix}$$

$$r_h = [-3.3526 \quad -1.0328 \quad -0.2724 \quad 0.6572 \quad -0.1576 \quad 0.9250]^\text{T}$$

$$\theta_j = [0.2891 \quad -1.0308]^\text{T}$$

$$w = \begin{bmatrix} 0.0798 & -0.1080 & -0.0044 & -0.7329 & 0.9450 & 0.2738 \\ -1.4042 & 0.0712 & -0.6059 & -0.4502 & 0.7257 & 0.0036 \end{bmatrix}$$

4. Conclusions

Based on the evaluation factors such as the geometric data of the substation panel, the stress performance, the fire resistance performance data, etc., a BP neural network, a method of machine learning, was used to establish the nonlinear relationship between panel performance stress and fire resistance under impact of fire. This model can quickly predict the performance of the substation panel under fire. The prediction of the thermal-mechanical coupling evaluation model is very close to the actual test, and satisfy the error

requirements. Additionally, the specimen was verified by numerical simulation. Comparing the neural network with numerical simulation, the result indicates the error of neural network prediction is about half smaller than that of numerical simulation, the prediction result of neural network is better than that of numerical simulation. The correctness and reliability of the thermal–mechanical coupling performance evaluation model is verified. If meeting the requirements of the test itself and the amount of data required by the structure of the neural network, the thermal–mechanical coupling evaluation model constructed in this study can be directly used for similar models. It does not need to conduct additional tests. As the types and quantities of data for training become richer, the models we build will become more and more refined. Therefore, this can provide a reference for exploring more thermal coupling evaluation models and complex functional relationships of materials based on neural networks under different loading modes in the future.

Author Contributions: Conceptualization, methodology, data curation, formal analysis; writing—review and editing, project administration, funding acquisition, Z.L.; conceptualization, methodology, supervision, project administration, funding acquisition, C.Z.; data curation, formal analysis, writing—original draft, preparation and editing, J.O.; data Curation, X.L.; data curation, Y.W.; data curation, X.W.; data curation, X.Z.; data curation, F.C.; data Curation, C.X., J.O. and X.L. contributed equally to this work and they are co-first authors of this article. All authors have read and agreed to the published version of the manuscript.

Funding: This research was funded by Science and Technology Project of Guangdong Power Grid Co., Ltd (037700KK52190022), the National Natural Science Foundation of China (NSFC) (Grant No.41977230), the National Key Research and Development Project (Grant No. 2017YFC1501203, No. 2017YFC1501201), the Special Fund Key Project of Applied Science and Technology Research and Development in Guangdong (Grant No. 2015B090925016, No. 2016B010124007).

Institutional Review Board Statement: The study did not require ethical approval.

Informed Consent Statement: Not applicable.

Data Availability Statement: Not applicable.

Acknowledgments: The authors would like to thank the anonymous reviewers for their very constructive and helpful comments.

Conflicts of Interest: The authors declare that they have no conflict of interest.

Appendix A

Table A1. Fire resistance and stress performance data of the panel.

Sample	Heating Time (min)	Average Furnace Temperature (°C)	Average Temperature of Backfire Surface (°C)	Pressure (Pa)	Time (s)	Bending Load (KN)
1	0	0	0	0	0.000	0
2	1	79.84	3.29	3.0577	1.798	0.0152
3	2	173.4	3.06	4.349	3.596	0.0619
4	3	267.91	3.12	5.4032	5.394	0.0949
5	4	360.6	4.9	5.8117	7.192	0.1097
6	5	433.88	2.36	5.1342	8.991	0.1888
7	6	468.52	3	11.858	10.789	0.287
8	7	504.38	2.5	6.7311	12.587	0.3562
9	8	535.65	1.09	8.499	14.385	0.4535
10	9	577.35	3.45	7.9913	16.183	0.5464

Table A1. Cont.

Sample	Heating Time (min)	Average Furnace Temperature (°C)	Average Temperature of Backfire Surface (°C)	Pressure (Pa)	Time (s)	Bending Load (KN)
11	10	625	2.94	10.133	17.981	0.6664
12	11	634.44	2.04	11.221	19.779	0.8527
13	12	643.43	1.94	9.6595	21.577	0.9194
14	13	664.89	1.28	11.8	23.375	1.0552
15	14	690.58	1.9	9.017	25.173	1.1762
16	15	705.34	3.27	11.87	26.972	1.2974
17	16	721.01	3.77	9.6982	28.770	1.4346
18	17	734.37	3.24	8.1376	30.568	1.5541
19	18	742.72	2.88	11.704	32.366	1.7039
20	19	750.87	2.65	12.759	34.164	1.8248
21	20	757.59	3.6	10.145	35.962	1.9602
22	21	763.69	3.13	12.014	37.760	2.114
23	22	773	2.27	13.136	39.558	2.3759
24	23	780.88	2.33	15.751	41.356	2.5796
25	24	794.49	3.52	12.086	43.154	2.7826
26	25	802.42	2.67	14.159	44.953	2.9971
27	26	809.7	2.96	16.672	46.751	3.2553
28	27	817.29	2.32	13.244	48.549	3.4676
29	28	828.68	1.68	11.989	50.347	3.659
30	29	840.37	4.26	11.958	52.145	3.8044
31	30	844.53	3.45	14.878	53.943	4.0017
32	31	851.16	3.73	17.732	55.741	4.3081
33	32	857.39	4.34	15.323	57.539	4.5063
34	33	854.14	5.18	13.932	59.337	4.6692
35	34	861.78	6.84	13.22	61.135	4.9182
36	35	867.05	3.7	12.95	62.934	5.1096
37	36	871.16	6.4	14.14	64.732	5.3131
38	37	876.67	5.2	18.894	66.530	5.4892
39	38	881.12	5.24	15.398	68.328	5.7004
40	39	884.83	4.83	14.108	70.126	5.8432
41	40	887.87	4.21	13.907	71.924	5.9585
42	41	889.97	2.81	13.67	73.722	6.0633
43	42	893	1.73	12.992	75.520	6.4429
44	43	898.57	1.2	12.621	77.318	6.692
45	44	900.57	1.55	13.437	79.116	6.9692
46	45	905.35	1.64	14.015	80.915	7.1593
47	46	908.14	3.61	13.948	82.713	7.3998
48	47	910.72	2.79	13.949	84.511	7.6056
49	48	914.22	2.12	13.951	86.309	7.9198

Table A1. Cont.

Sample	Heating Time (min)	Average Furnace Temperature (°C)	Average Temperature of Backfire Surface (°C)	Pressure (Pa)	Time (s)	Bending Load (KN)
50	49	914.51	4.92	13.954	88.107	8.1175
51	50	919.4	3.94	13.989	89.905	8.3583
52	51	922.69	6.19	14.364	91.703	8.634
53	52	925.51	6.38	14.84	93.501	8.8009
54	53	929.22	6.44	14.399	95.299	9.002
55	54	933.64	7.51	14.027	97.097	9.2243
56	55	938.97	9.24	14.843	98.896	9.3998
57	56	942.03	11.24	16.543	100.694	9.5576
58	57	944.37	12.45	18.004	102.492	9.7716
59	58	947.88	14.54	16.851	104.290	9.937
60	59	944.27	17.79	13.966	106.088	10.116
61	60	947.25	15.6	13.934	107.886	10.237
62	61	949.48	13.49	14.342	109.684	10.439
63	62	952.08	13.32	15.022	111.482	10.679
64	63	954.15	16.91	16.586	113.280	10.9
65	64	955.83	19.37	17.402	115.078	11.103
66	65	958.84	18.06	18.863	116.877	11.379
67	66	962.18	21.68	15.877	118.675	11.6
68	67	966.24	20.39	14.384	120.473	11.794
69	68	969.58	20.66	13.91	122.271	12.07
70	69	967.65	21.86	14.387	124.069	12.231
71	70	970.98	19.67	16.629	125.867	12.374
72	71	973.61	23.63	16.834	127.665	12.742
73	72	976.41	24.6	16.088	129.463	12.884
74	73	978.48	26.5	14.731	131.261	13.016
75	74	978.69	28.38	14.053	133.059	13.21
76	75	981.34	29.56	16.432	134.858	13.381
77	76	982.55	31.64	18.029	136.656	13.548
78	77	983.33	31.82	18.777	138.454	13.693
79	78	986	32.33	17.387	140.252	13.835
80	79	985.67	37.18	13.891	142.050	13.985
81	80	986.19	34.77	15.217	143.848	14.102
82	81	987.83	37.34	16.949	145.646	14.218
83	82	989.37	38.31	17.731	147.444	14.448
84	83	992.76	40.21	14.677	149.242	14.555
85	84	997.82	43.91	13.965	151.040	14.666
86	85	999.42	42.37	15.563	152.839	14.86
87	86	1001.8	47.47	16.311	154.637	15.123
88	87	1004	47.86	17.738	156.435	15.303

Table A1. Cont.

Sample	Heating Time (min)	Average Furnace Temperature (°C)	Average Temperature of Backfire Surface (°C)	Pressure (Pa)	Time (s)	Bending Load (KN)
89	88	1005.8	50.86	16.551	158.233	15.469
90	89	1009.2	52.06	14.923	160.031	15.585
91	90	1006.1	45.67	16.52	161.829	15.71
92	91	1007.6	46.3	17.301	163.627	15.968
93	92	1008.8	48.17	16.862	165.425	16.002
94	93	1011.3	50.79	16.047	167.223	16.039
95	94	1013	55.77	15.029	169.021	16.167
96	95	1014.3	55.85	14.896	170.820	16.339
97	96	1016.1	57.01	15.814	172.618	16.428
98	97	1017.8	58.17	14.865	174.416	16.512
99	98	1020.6	56.41	14.865	176.214	16.596
100	99	1020.3	56.48	14.935	178.012	16.681
101	100	1022.5	58.42	16.329	179.810	16.74
102	101	1025.1	53.55	17.756	181.608	16.865
103	102	1026.3	56.35	15.992	183.406	16.986
104	103	1028.8	58.47	15.757	185.204	17.071
105	104	1029.3	61.61	17.863	187.002	17.123
106	105	1031.7	58.83	15.589	188.801	17.229
107	106	1031.5	60.25	14.911	190.599	17.369
108	107	1034.3	60.88	16.814	192.397	17.487
109	108	1036.5	60.93	14.881	194.195	17.605
110	109	1035.1	64.07	14.881	195.993	17.577
111	110	1037.6	65.42	16.92	197.791	17.662
112	111	1037.8	60	15.529	199.589	17.877
113	112	1038.9	58.92	14.885	201.387	17.853
114	113	1040.1	58.82	17.807	203.185	17.876
115	114	1042.2	58.58	15.499	204.983	17.968
116	115	1042.9	60.23	14.923	206.782	18.081
117	116	1043.3	59.86	16.86	208.580	18.181
118	117	1045.1	59.06	14.858	210.378	18.182
119	118	1046.5	58.54	16.83	212.176	18.27
120	119	1045.9	60.74	16.83	213.974	18.366
121	120	1047.3	64.13	16.83	215.772	18.392
122	121	1048.9	58.24	14.897	217.570	18.488
123	122	1051	58.63	17.819	219.368	18.58
124	123	1052.8	59.49	15.749	221.166	18.639
125	124	1054.6	59.2	14.052	222.964	18.655
126	125	1055.7	60.53	14.97	224.763	18.733
127	126	1057.5	60.28	15.006	226.561	18.916

Table A1. Cont.

Sample	Heating Time (min)	Average Furnace Temperature (°C)	Average Temperature of Backfire Surface (°C)	Pressure (Pa)	Time (s)	Bending Load (KN)
128	127	1058.9	58.28	19.863	228.359	18.961
129	128	1060.6	57.76	15.857	230.157	18.998
130	129	1060.7	57	16.98	231.955	19.101
131	130	1063.2	57.95	16.98	233.753	19.139
132	131	1064.8	58.31	15.963	235.551	19.271
133	132	1066.1	57.56	17.866	237.349	19.345
134	133	1068.7	58.53	15.933	239.147	19.469
135	134	1066.8	58.26	18.854	240.945	19.456
136	135	1069.3	58.71	16.037	242.744	19.544
137	136	1070.3	58.68	16.853	244.542	19.677
138	137	1070.7	58.49	17.941	246.340	19.674
139	138	1072	58.11	15.973	248.138	19.672
140	139	1071.6	58.5	16.891	249.936	19.815
141	140	1073.3	59.79	15.738	251.734	19.827
142	141	1074	60.42	14.925	253.532	19.85
143	142	1077.2	59.75	15.367	255.330	19.961
144	143	1075.3	58.78	16.999	257.128	20.132
145	144	1077.2	59.56	16.185	258.926	20.111
146	145	1077.1	59.34	15.405	260.725	20.281
147	146	1077.6	60.26	14.863	262.523	20.4
148	147	1078	58.89	16.935	264.321	20.36
149	148	1077.2	60.51	15.918	266.119	20.547
150	149	1079.2	63.73	17.923	267.917	20.555
151	150	1081.2	61.49	15.921	269.715	20.593
152	151	1083.1	58.71	17.925	271.513	20.787
153	152	1086	58.99	15.991	273.311	20.758
154	153	1085.5	59.37	17.962	275.109	20.805
155	154	1087.8	59.31	15.892	276.907	20.912
156	155	1090	59.96	15.895	278.706	21.004
157	156	1090.9	59.23	15.895	280.504	21.061
158	157	1092.7	58.71	15.895	282.302	21.038
159	158	1089.6	58.42	15.93	284.100	21.135
160	159	1093.5	58.03	15.933	285.898	21.264
161	160	1095.2	60.64	15.933	287.696	21.275
162	161	1096.7	58.66	16.818	289.494	21.257
163	162	1098.2	58.48	15.868	291.292	21.402
164	163	1096	57.96	15.868	293.090	21.405
165	164	1098.5	58.82	15.868	294.888	21.443

Table A1. Cont.

Sample	Heating Time (min)	Average Furnace Temperature (°C)	Average Temperature of Backfire Surface (°C)	Pressure (Pa)	Time (s)	Bending Load (KN)
166	165	1099.2	60.62	15.868	296.687	20.986
167	166	1099.9	59.08	15.943	298.485	20.603
168	167	1101.3	58.55	15.946	300.283	20.502
169	168	1099	59.65	15.946	302.081	20.263
170	169	1101	58.56	15.946	303.879	19.9
171	170	1101.8	61.27	17.916	305.677	19.858
172	171	1102.2	57.09	15.982	307.475	19.903
173	172	1102.4	56.92	19.039	309.273	19.868
174	173	1102.4	57.55	17.783	311.071	19.913
175	174	1104.5	58.75	15.985	312.869	19.827
176	175	1105	58.93	15.037	314.668	19.665
177	176	1106.2	60.01	16.871	316.466	19.445
178	177	1107	60.76	16.975	318.264	19.301
179	178	1107.5	60.35	18.946	320.062	19.131
180	179	1107.9	61.09	16.06	321.860	18.953
181	180	1108.2	61.39	19.016	323.658	18.834
182	181	1089.3	61.3	16.809	325.456	18.664
183	182	1089.2	61.44	10.868	327.254	16.174
184	183	1010.7	61.69	10.19	329.052	12.114

References

1. Hazel, T.; Norris, A.; Barbizet, M.; Et, A. Designing prefabricated substation buildings according to GOST standards; Record of Conference Papers; Industry Applications Society; Forty-Ninth Annual Conference. In Proceedings of the 2002 Petroleum and Chemical Industry Technical Conference, New Orleans, LA, USA, 23–25 September 2002; pp. 251–259.
2. Zhengmao, F.; Xiuhua, S.; Hongzhi, C.; Et, A. Optimization design of box structure for prefabricated substation. *Int. J. Res. Eng. Technol.* **2018**, *7*, 85–90.
3. Zou, P.L. Comparative analysis of traditional civil construction new energy substation and modular prefabricated cabin substation. *Mech. Electr. Inf.* **2020**, *38*, 9.
4. Gerges, M.; Demian, P.; Adamu, Z. Customising Evacuation Instructions for High-Rise Residential Occupants to Expedite Fire Egress: Results from Agent-Based Simulation. *Fire* **2021**, *4*, 21. [\[CrossRef\]](#)
5. Ghodrat, M.; Shakeriaski, F.; Nelson, D.J.; Simeoni, A. Existing Improvements in Simulation of Fire–Wind Interaction and Its Effects on Structures. *Fire* **2021**, *4*, 27. [\[CrossRef\]](#)
6. Ali, F.; Nadjai, A.; Silcock, G.; Et, A. Outcomes of a major research on fire resistance of concrete columns. *Fire Saf. J.* **2004**, *39*, 433–445. [\[CrossRef\]](#)
7. Kodur, V.K.R.; Dwaikat, M.M.S.; Dwaikat, M.B. High-temperature properties of concrete for fire resistance modeling of structures. *ACI Mater. J.* **2008**, *105*, 517–527.
8. Ran, L.; Zhao, H.; Huang, W.; Li, X.; Wang, Y.; Hu, Y. Fire resistance analysis of door and wall composite components. *Fire Sci. Technol.* **2014**, *33*, 1031–1033.
9. Serrano, R.; Cobo, A.; Prieto, M.I.; Et, A. Analysis of fire resistance of concrete with polypropylene or steel fibers. *Constr. Build. Mater.* **2016**, *122*, 302–309. [\[CrossRef\]](#)
10. Tian, J.; Zhu, P.; Qu, W. Study on fire resistance time of hybrid reinforced concrete beams. *Struct. Concr.* **2019**, *20*, 1941–1954. [\[CrossRef\]](#)
11. Naser, M.Z.; Kodur, V.K.R. Comparative fire behavior of composite girders under flexural and shear loading. *Thin-Walled Struct.* **2017**, *116*, 82–90. [\[CrossRef\]](#)
12. Hawileh, R.A.; Naser, M.Z. Thermal-stress analysis of RC beams reinforced with GFRP bars. *Compos. Part B Eng.* **2012**, *43*, 2135–2142. [\[CrossRef\]](#)

13. Hawileh, R.A.; Naser, M.; Zaidan, W.; Al, E. Modeling of insulated CFRP-strengthened reinforced concrete T-beam exposed to fire. *Eng. Struct.* **2009**, *31*, 3072–3079. [\[CrossRef\]](#)
14. Hawileh, R.A.; Naser, M.; Zaidan, W.; Al, E. Transient Thermal-Stress Finite Element Analysis of CFRP Strengthened RC beams Exposed to different Fire Scenarios. *Mech. Adv. Mater. Struc.* **2011**, *18*, 172–180. [\[CrossRef\]](#)
15. Aguado, J.V.; Alberro, V.; Espinos, A.; Al, E. A 3D finite element model for predicting the fire behavior of hollow-core slabs. *Eng. Struct.* **2016**, *108*, 12–27. [\[CrossRef\]](#)
16. Faridmehr, I.; Nikoo, M.; Baghban, M.H.; Pucinotti, R. Hybrid Krill Herd-ANN Model for Prediction Strength and Stiffness of Bolted Connections. *Buildings* **2021**, *11*, 229. [\[CrossRef\]](#)
17. Avossa, A.M.; Picozzi, V.; Ricciardelli, F. Load-Carrying Capacity of Compressed Wall-Like RC Columns Strengthened with FRP. *Buildings* **2021**, *11*, 285. [\[CrossRef\]](#)
18. Abd-Elhamed, A.; Shaban, Y.; Mahmoud, S. Predicting Dynamic Response of Structures under Earthquake Loads Using Logical Analysis of Data. *Buildings* **2018**, *8*, 61. [\[CrossRef\]](#)
19. Mishra, P.; Samui, P.; Mahmoudi, E. Probabilistic Design of Retaining Wall Using Machine Learning Methods. *Appl. Sci.* **2021**, *11*, 5411. [\[CrossRef\]](#)
20. Jain, N.; Bansal, V.; Virmani, D.; Gupta, V.; Salas-Morera, L.; Garcia-Hernandez, L. An Enhanced Deep Convolutional Neural Network for Classifying Indian Classical Dance Forms. *Appl. Sci.* **2021**, *11*, 6253. [\[CrossRef\]](#)
21. Wu, M.; Wang, J. Estimating Contact Force Chains Using Artificial Neural Network. *Appl. Sci.* **2021**, *11*, 6278. [\[CrossRef\]](#)
22. Jiao, Z.; Hu, P.; Xu, H.; Al, E. Machine learning and deep learning in chemical health and safety: A systematic review of techniques and applications. *ACS Chem. Health Saf.* **2020**, *27*, 316–334. [\[CrossRef\]](#)
23. Wang, W.; Kiik, M.; Peek, N.; Al, E. A systematic review of machine learning models for predicting outcomes of stroke with structured data. *PLoS ONE* **2020**, *15*, e234722.
24. Abuodeh, O.R.; Abdalla, J.A.; Hawileh, R.A. Prediction of shear strength and behavior of RC beams strengthened with externally bonded FRP sheets using machine learning techniques. *Compos. Struct.* **2020**, *234*, 111698. [\[CrossRef\]](#)
25. Abuodeh, O.; Abdalla, J.A.; Hawileh, R.A. Prediction of compressive strength of ultra-high performance concrete using SFS and ANN. In Proceedings of the 2019 8th International Conference on Modeling Simulation and Applied Optimization (ICMSAO), Sanya, China, 9–10 November 2019; pp. 1–5.
26. Liu, T.; Wang, Z.; Zeng, J.; Al, E. Machine-learning-based models to predict shear transfer strength of concrete joints. *Eng. Struct.* **2021**, *249*, 113253. [\[CrossRef\]](#)
27. Chen, C.S.; Tzeng, Y.M.; Hwang, J.C. The application of artificial neural networks to substation load forecasting. *Electr. Power Syst. Res.* **1996**, *38*, 153–160. [\[CrossRef\]](#)
28. Hsu, Y.Y.; Lu, F.C. A combined artificial neural network-fuzzy dynamic programming approach to reactive power/voltage control in a distribution substation. *IEEE Trans. Power Syst.* **1998**, *13*, 1265–1271.
29. Borkowski, D.; Wetula, A.; Bień, A. Contactless measurement of substation busbars voltages and waveforms reconstruction using electric field sensors and artificial neural network. *IEEE Trans. Smart Grid* **2014**, *6*, 1560–1569. [\[CrossRef\]](#)
30. Nguyen, B.N.; Quyen, A.H.; Nguyen, P.H.; Al, E. Wavelet-based Neural Network for recognition of faults at NHABE power substation of the Vietnam power system. In Proceedings of the 2017 International Conference on System Science and Engineering (ICSSE), Ho Chi Minh City, Vietnam, 21–23 July 2017; pp. 165–168.
31. Dudzik, M.; Jagiello, A.; Drapik, S.; Et, P.J. The selected real tramway substation overload analysis using the optimal structure of an artificial neural network. In Proceedings of the 2018 International Symposium on Power Electronics, Electrical Drives, Automation and Motion (SPEEDAM), Amalfi, Italy, 20–22 June 2018; pp. 413–417.
32. Da Silva, A.P.A.; Insfran, A.H.F.; Da Silveira, P.M.; Et, A. Neural networks for fault location in substations. *IEEE Trans. Power Deliv.* **1996**, *11*, 234–239. [\[CrossRef\]](#)
33. Wang, J.; You, Z.; Xiao, J.; Tan, Z. Deep learning based state recognition of substation switches. In Proceedings of the AIP Conference Proceedings, Kuala Lumpur, Malaysia, 24–26 July 2018; p. 1971.
34. Jiang, H.; Liu, S.; Zhou, J.; Zhu, G.; Wang, K.; Shi, Z. Adaptive Noise Reduction of Transformer in Substation Based on Genetic Wavelet Neural Network. *Electr. Power Sci. Eng.* **2020**, *36*, 25–31.
35. Oliveira, B.A.S.; Neto, A.P.D.F.; Fernandino, R.M.A.; Et, A. Automated Monitoring of Construction Sites of Electric Power Substations Using Deep Learning. *IEEE Access* **2021**, *9*, 19195–19207. [\[CrossRef\]](#)
36. Wang, L.; Zeng, Y.; Chen, T. Back propagation neural network with adaptive differential evolution algorithm for time series forecasting. *Expert Syst. Appl.* **2015**, *42*, 855–863. [\[CrossRef\]](#)
37. Li, J.; Cheng, J.; Shi, J.; Al, E. Brief introduction of back propagation (BP) neural network algorithm and its improvement. In *Advances in Computer Science and Information Engineering*; Springer: Berlin/Heidelberg, Germany, 2012.
38. Singh, A.K.; Kumar, B.; Singh, S.K.; Al, E. Multiple watermarking technique for securing online social network contents using back propagation neural network. *Future Gener. Comput. Syst.* **2018**, *86*, 926–939. [\[CrossRef\]](#)
39. Fire-Resistance Tests—Elements of Building Construction—Part 1: General Requirements (GB/T 9978.1-2008). Available online: <https://gf.1190119.com/list-704.htm> (accessed on 15 November 2021).
40. Fire-Resistance Tests—Elements of Building Construction—Part 8: Specific Requirements for Non-Loadbearing Vertical Separating Elements (GB/T 9978.8-2008). Available online: <https://www.doc88.com/p-7798292250942.html> (accessed on 15 November 2021).